

NUMERICAL SIMULATION OF TURBULENT FLOW IN CORRUGATED PIPES

Henrique S. de Azevedo, rique.stel@gmail.com
Rigoberto E. M. Morales, rmorales@utfpr.edu.br
Admilson T. Franco, admilson@utfpr.edu.br
Silvio L. M. Junqueira, silvio@utfpr.edu.br
Raul H. Erthal, rherthal@utfpr.edu.br

DAMEC/UTFPR, Av. Sete de Setembro 3165, CEP. 80230-901, Curitiba-PR-Brasil

Marcelo de Albuquerque Lima Goncalves, marcelog@petrobras.com.br

PDP/TE/CENPES/PETROBRAS, Av. Jequitibá s/n, Ilha do Fundão, Qdra 7, CEP. 21941-598, Rio de Janeiro-RJ-Brasil

Abstract. *Corrugated pipes are used in various engineering applications such heat exchangers and oil transport. In most cases these pipes consist of periodically distributed grooves at the duct inner wall. Numerical and experimental works reported the influence of grooves height and length in the turbulent flow by inspection of several turbulent properties such as velocity fluctuations and Reynolds stress. The present article aims to investigate the influence of grooves height and length in the global friction factor of turbulent flow through periodically corrugated pipes. Mass and momentum conservation equations are revised and specific boundary conditions are set to characterize a periodic fully developed regime in a single axisymmetric bidimensional module which represents the periodically corrugated duct geometry. The set of algebraic equations is discretized through the Finite Volume Method, with the Hybrid interpolation scheme applied to the convective terms, and solved using the commercial software PHOENICS CFD. The simulation of turbulent, incompressible, isothermal and single-phase flow is considered. The algebraic turbulence model LVEL is used. Four geometric configurations are assumed, including grooves height and length variations, in order to compare their influence on the friction factor. The obtained numerical friction factors show good agreement with previous experimental results, specially for Reynolds numbers over 20000. Numerical results for corrugated pipes compared to the Blasius smooth pipe correlation shows that the friction factor increases compared to smooth pipes, and such increase is more significant for higher Reynolds numbers and for larger grooves as well. These trends appear to be related to an enhancement of the momentum transport over the corrugated wall due to the recirculating pattern inside the grooves, in accordance with previous experimental works.*

Keywords: *corrugated pipes, friction factor, numerical simulation, Finite Volume Method.*

1. INTRODUCTION

Corrugated walls can be described as rough surfaces consisting of discrete grooves periodically disposed along the flow direction, and have been studied for many years, much because of their large use in many engineering devices. These studies are carried on many aspects, as heat transfer enhancement, drag reduction, among others.

Many years later than the work of Nikuradse (1933) on homogeneous sand grain roughness, Perry et al. (1969) held one of the first theoretical studies concerning turbulent flow in discrete rough walls. Among many other contributions, Perry et al. (1969) proposed a geometric denomination for the discrete corrugated elements based upon the roughness length scale related to the flow, as shown in Fig. 1. According to the same authors, for square cavities, Fig. 1-(a), stable turbulent vortices are confined inside de cavities, isolating the outer flow from the roughness; the appropriate roughness length scale of the flow in this configuration becomes the boundary layer thickness, δ , which has the order of magnitude of the pipe diameter, d , in internal flows. For this reason, Perry et al. (1969) denominate surfaces with square rough cavities as “ d -type” rough walls. Conversely, cavities with large lengths in respect to the cavity height, Fig. 1-(b), cannot sustain stable vortices, and the outer flow reattach in the bottom of the cavity; in this configuration, the outer flow is then exposed to the ribs, and the boundary layer thickness is no longer an appropriate roughness length scale. Now, the cavity height, k , is clearly the appropriate roughness length scale since it plays a much more important role in describing the wall roughness. Because of this analysis, Perry et al. (1969) classify cavities with large lengths in respect to the rib height as “ k -type” roughness, and these two denominations have been widely used ever since.

Several works followed Perry et al. (1969) on the analysis of “ d ” and “ k ” type roughness characteristics. Chen et al. (1986) made an experimental study of turbulent air flow in channels with corrugated walls. The main focus were investigate the possibility of drag reduction in turbulent flows at low Reynolds numbers associated with the capability of various corrugation configurations (such as triangular, trapezoidal and “ d -type” square forms) in retaining stable vortices and avoiding propagation of turbulent bursts throughout the flow. In fact, the work of Chen et al. (1986) emerges of previous observations (Liu et al. [1966], Kennedy et al. [1973] and Walsh & Weinstein [1979]) in which was proposed that drag reduction is possible if the dimensionless height, h^+ , and pitch, S^+ , of the cavities were kept under 25 and 100, respectively, with h^+ and S^+ given by $h^+ = hV_* / \nu$ and $S^+ = hV_* / \nu$, where h and S are the

height and pitch of the cavities, V_* is the friction velocity and ν is the cinematic viscosity. Chen et al. (1986) found that for Reynolds numbers under 16000 triangular and trapezoidal corrugation forms with $h^+ \approx 20$ and $S^+ \approx 83$ are capable of reducing the global friction factor, in comparison with that calculated for a channel with smooth walls. For $h^+ \approx 32$ and still keeping $S^+ < 100$, the friction factor tended to be higher than that calculated for smooth wall channels.

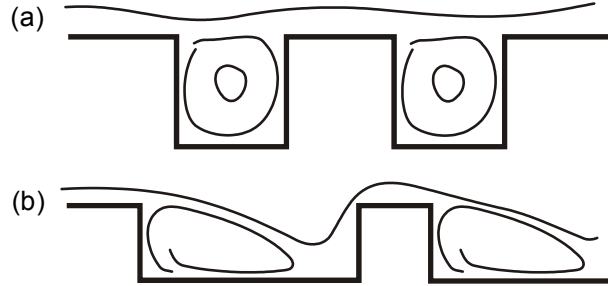


Figure 1. Geometry of “d-type” (a) and “k-type” (b) roughness, flow from left to right. (Font: Jiménez [2004], p. 181).

Djenidi et al. (1994), using Laser-Doppler Anemometry, studied the flow over a flat plate with “d-type” roughness. The structure of the external flow over a flat plate provided by Djenidi et al. (1994) where a specially designed configuration which allowed the visualization of the vortices behavior inside de “d-type” grooves. The main visual observation of Djenidi et al. (1994) was that, confronting Perry et al. (1969), “d-type” grooves do not entirely isolate de outer flow from the roughness effects. Conversely, there are strong ejections originated in the cavity’s confined vortex expelled right to the outer flow, which happens at a time scale close to $5.5\delta/U_\infty$, where U_∞ is the bulk velocity. Generally speaking, these ejections represent an average enhancement of momentum transfer from the cavity to the outer flow, and according to Djenidi et al. (1994) this effect causes global increases in turbulent intensities near the wall, including other entities, namely, the Reynolds shear stress, the friction coefficient and thus the average pressure drop along the corrugated wall.

Not just on the form of the cavity, many works investigate the behavior of the friction factor for discrete roughness elements helically distributed at the pipe wall along the flow direction. In this field, Silberman (1970) proposed that is it possible to reduce drag in helically corrugated pipes (consisting of cavities with a length of the same order of magnitude of the ribs height) decreasing the helix angle (i.e. disposing ribs more inclined in the flow direction), and later Silberman (1980) demonstrated his previous proposed trend as being correct. On the other hand, Dong et al. (2001) showed that spirally corrugated pipes with cavities much larger than the rib height tend to increase the global friction factor in comparison with smooth pipes.

More recently, Morales et al. (2007) held an experimental study in turbulent flow in “d-type” corrugated pipes, with both straight and single-start helical grooves. The experimental loop constructed at the LACIT - Thermal Science Laboratory of UTFPR - Federal Technological University - Paraná (Morales et al., 2007) was designed to provide turbulent water flow in 1 inch diameter pipes, and the obtained data showed that the global friction factor increases in corrugated pipes in relation to smooth pipes.

In light of the wide applicability of these results, with special interest in several industrial devices and optimization of oil transport processes, the present paper develops a numerical study of the turbulent flow in corrugated pipes. The numerical simulation of the single phase, isothermal and incompressible flow is done using CFD, through the commercial software PHOENICS CFD (Spalding, 1994). The influence of the geometric characteristics of the corrugate on the friction factor is carried out evaluating four different configurations involving aspect ratios of the grooves and six Reynolds numbers. The numerical results obtained for one out of four configurations are validated with experimental data obtained by Morales et al. (2007).

2. MATHEMATICAL AND NUMERICAL MODELING

Incompressible and isothermal fluid flow in pipes is governed by mass and momentum conservation equations, and in the present work these equations are solved for turbulent flow utilizing the algebraic LEVEL turbulence model, detailed by Spalding (1994). In the conservative generalized form for steady flow, these conservation equations are given by:

$$\nabla \cdot (\rho \vec{V} \phi) = \nabla \cdot (\Gamma \nabla \phi) + S, \quad (1)$$

where ρ is the fluid density, $\phi=1$ and $\Gamma=S=0$ for continuity and $\phi=\vec{V}$, $\Gamma=\mu_{eff}$ (effective dynamic viscosity) and $S=-\nabla p$ for momentum equations, in the absence of body forces. The zero-equation LEVEL turbulence model (Spalding, 1994) employs an algebraic equation for the evaluation of the turbulent dynamic viscosity, μ_t as follows:

$$\mu_t = \mu \cdot \left(\frac{\kappa}{E} \right) \cdot \left[e^{\kappa u^+} - 1 - \kappa u^+ - \frac{(\kappa u^+)^2}{2} - \frac{(\kappa u^+)^3}{6} \right], \quad (2)$$

where u^+ is the dimensionless velocity parallel to the wall, $u^+ = u/V^*$, κ is the von Karman constant, $\kappa = 0.417$ and E is another constant ($E = 8.6$). The effective dynamic viscosity μ_{eff} used in Eq. (1) is the sum of the turbulent flow viscosity and the fluid dynamic viscosity, $\mu_{eff} = \mu_t + \mu$.

Although these governing equations, together with adequate boundary conditions, represent a complete description of the considered problem, some convenient assumptions must be made in order to optimize the solution domain, avoiding excessive computational effort to solve a long corrugated duct with several grooves. This is made through the periodic fully developed facility, and its basic concepts, followed by its adequate numerical implementation, are described in this section.

2.1. The periodic fully developed regime

Corrugated pipes are cylindrical ducts with periodically distributed grooves at the wall, and can be solved as a single corrugated domain subject to a periodic fully developed flow, as described by Patankar et al. (1977). Figure 2 shows a schematic representation of a corrugated pipe, in which one can easily note that each module, indicated in Fig. 2 with dashed lines, repeats itself in identical fashion along the duct.

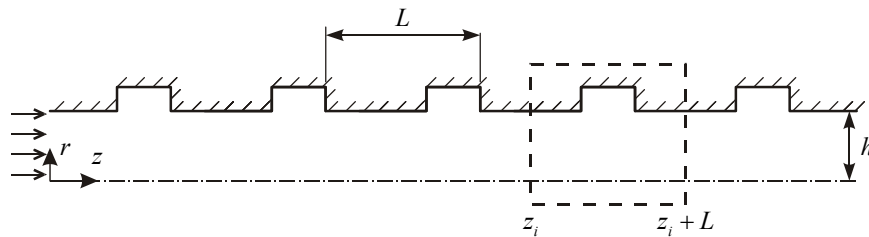


Figure 2. Geometrical scheme for the corrugated pipe analyzed.

As detailed by Patankar et al. (1977), it is assumed that the individualized module is far enough from the entrance region that the flow field becomes identical in each module. This analysis carries to the following periodic boundary condition for v and w velocities (radial and axial components, respectively):

$$v(r, z_i) = v(r, z_i + L), \quad w(r, z_i) = w(r, z_i + L) \quad (3)$$

These rather simple boundary conditions cannot be applied to the pressure, p . However, the pressure gradient experiences itself a periodic condition, because far from the entrance region the periodic condition guarantees that, in each module, the condition $p(r, z_i) - p(r, z_i + L) = p(r, z_i + L) - p(r, z_i + 2L) = \dots$ is valid. Because of this periodic behavior, pressure p is divided in two components:

$$p(r, z) = -\beta z + P(r, z), \quad (4)$$

where the first one, $-\beta z$ represents an overall linear decay of pressure and the second one, $P(r, z)$ stands for a periodic pressure, which stores all possible pressure variations throughout the module. The pressure gradient terms $-\partial p / \partial r$ and $-\partial p / \partial z$ in momentum conservation equations are then changed using Eq. (4), resulting in a new source term in z -direction momentum equation, β , and new pressure gradient terms to be solved with momentum equations, $-\partial P / \partial r$ and $-\partial P / \partial z$. Note that, now, $P(r, z)$ is the solved variable, instead of the real pressure $p(r, z)$.

Since β stands for a constant term which represents the module's global pressure gradient, Eq. (4) indicates that the periodic pressure $P(r, z)$ must repeat itself in each module, and then the third relevant boundary condition for the problem is:

$$P(r, z_i) = P(r, z_i + L) = P(r, z_i + L) = \dots \quad (5)$$

Equations (3) and (5) describe the required boundary conditions for v , w and P in the flow axial direction, z . In the radial direction, r , no-slip condition at pipe wall and symmetry condition at pipe center line require that (see Fig. 2):

$$v(h, z) = w(h, z) = 0, \quad v(0, z) = 0, \quad \frac{\partial w(0, z)}{\partial r} = 0 \quad (6)$$

Mass and momentum conservation equations, together with the Zero Equation LEVEL turbulence model (Spalding, 1994) and boundary conditions described in Eqs. (3), (5) and (6) represent a complete mathematical description for the periodic fully developed flow in corrugated pipes. Since the flow is periodic fully developed, and not purely fully developed, important convective and diffusive terms in the momentum equations cannot be vanished, which leads to a complex system of non-linear differential partial equations to be solved. Therefore, a numerical solution is needed, and the Finite Volume Method described by Patankar (1980) is used. The most relevant considerations in this approach are made in sub-section 2.3. Before treating the problem numerically, however, it is interesting to define the geometrical domain to be further considered, which results from the assumption of periodic fully developed flow.

2.2. Geometrical modeling

As already previously proposed in the present work, four different configurations are assumed for the corrugated pipe, involving grooves height and length. Figure 3 shows the representative dimensions of the corrugated pipe, and their values are reported in Tab. 1 for the four configurations considered, where a is the grooves spacing, b is the groove length, c is the groove height, s is the pitch between two consecutive grooves and D is the pipe inner diameter, which is the same for each configuration considered, $D = 0.1$ m.

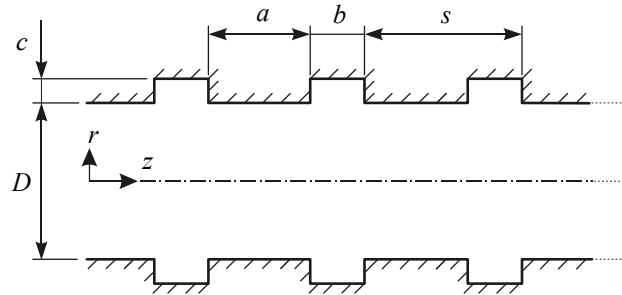


Figure 3. Main dimensions of the corrugated pipe.

Table 1. Numerical values of the main dimensions shown in Fig. 3, for the four geometric configurations assumed.

Configuration	a/D	b/D	c/D	s/D
1	0.11	0.015	0.03	0.125
2	0.11	0.03	0.03	0.14
3	0.11	0.04	0.03	0.15
4	0.11	0.04	0.04	0.15

The values assumed in Tab. 1 are chosen in this manner for the investigation of two effects: from configuration 1 to 3, the groove length b is increased, with the groove height c kept constant, in order to verify the influence of the groove length on the friction factor; from configuration 3 to 4, the groove length is kept constant instead, and the groove height c is increased, revealing any influence of variations in the groove height on the friction factor. Also, configuration 4 matches, in appropriate scale, with that used by Morales *et al.* (2007), for further validation.

From Fig. 3, it can be seen that the corrugated pipe considered is symmetric, and then it isn't necessary to solve the problem along the whole tangential direction. Thus, only a "sliced" tangential portion of the domain is needed (intrinsically indicating that the flow is essentially two-dimensional), as shown in Fig. 4. Furthermore, the periodic fully developed flow assumption allows the problem to be solved for a single module, similarly as the one marked by dashed

lines in Fig. 2. However, in order to avoid any possible numerical errors by not considering the influence of one groove in another subsequent one, a periodic geometric configuration consisting of two grooves (instead of one) is considered, as shown in Fig. 4. Note that the numerical domain remains still periodic (all the mathematical description of the subsection 2.1 are then still valid), but the numerical domain becomes presumably more reliable for turbulent flows than that one with just one groove.

2.3. Numerical considerations

Governing equations (1) are discretized using the Finite Volume Method (Patankar, 1980), and the Hybrid scheme is used to interpolate of the convective terms. The SIMPLEST algorithm, which stands for Semi-Implicit Method for Pressure-Linked Equations Shortened (Spalding, 1994), is used to the pressure-velocity coupling. The set of algebraic equations are solved through the commercial software PHOENICS CFD (Spalding, 1994).

A non-uniform orthogonal grid is used for the cylindrical-polar coordinate system, with grid refinement near the wall. The adequate number of control volumes in each sub-region of the pipe was obtained through a mesh test, in which the adequate number of control volumes is determined in order to represent the physical problem without increasing excessively in the computational time (in fact, it was found that the friction factor has a relatively low dependence on the mesh, varying less than 1% for grids finer than a 75×60 mesh). Figure 5 shows a schematic representation of the non-uniform grid distribution inside the groove, where the mesh configuration is more important. Note that the grid is more refined near the cavity corners, where is it expected that the more representative gradients will take place.

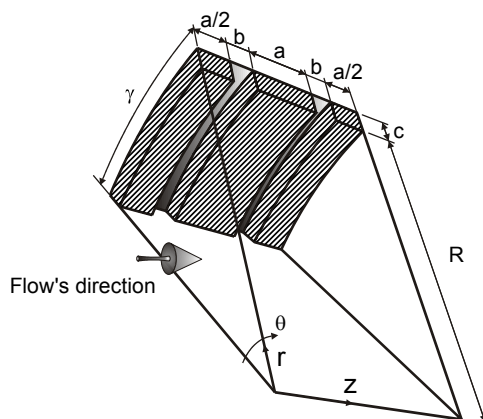


Figure 4. Schematic approach with two grooves for the numerical periodic domain of the corrugated pipe.

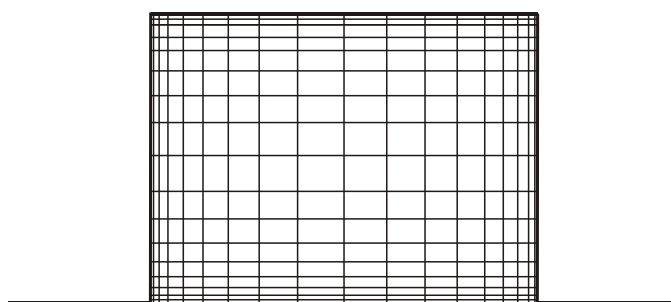


Figure 5. Grid distribution inside the corrugation cavity.

3. NUMERICAL SIMULATIONS – RESULTS AND DISCUSSIONS

This section brings the numerical results obtained for the four geometric configurations proposed, as well as relevant physical interpretations related to the observed turbulent flow pattern. The fluid properties assumed are density $\rho = 1000 \text{ kg/m}^3$ and cinematic viscosity $\nu = 1 \times 10^{-6} \text{ m}^2/\text{s}$, and the Reynolds numbers 6000, 10000, 20000, 30000, 40000 and 50000 are simulated.

3.1. Flow pattern

In general, works involving turbulent flow over surfaces with discrete roughness seek, directly or not, to associate measured changes in the flow's parameters with the flow's physical pattern observed. The work of Djenidi *et al.* (1994)

is an example of this fact, as discussed in section 1, where the aim was investigate the interaction between the vortices inside the grooves and the outer flow as a mechanism capable of changing turbulent properties.

Figure 6 shows examples of the general flow patterns of the confined vortex inside the groove observed in the present work, detailed here for Reynolds numbers 10000, Fig. 6-(a), and 50000, Fig. 6-(b). It can be observed, through Figs. 6-(a) and 6-(b), that the recirculation pattern inside the groove is influenced significantly by the Reynolds number. Note that in Fig. 6-(a), where the Reynolds number is somewhat low, the confined vortex is stable, and the interface region between the groove and the outer flow shows predominantly axial velocity components. On the other hand, Fig. 6-(b) shows that for higher Reynolds numbers the vortex center is slightly dislocated in comparison with the previous one. This can be assigned by an increase in the vortex intensity inside the groove, since flow's inertia for $Re = 50000$ is obviously higher than $Re = 10000$. As a consequence of this effect, the confined vortex is much less stable than the one observed for $Re = 10000$, and the intensified recirculation inside the groove causes the fluid to try to leave the cavity right to the outer flow, as a perturbation mechanism. In other words, the average effect of this pattern can be recognized as an enhancement in momentum transfer between the grooves and the outer flow associated with the increase in the Reynolds number. Not visually shown here, but also expected, the increase of the interface length, i.e. the increase of groove length, would cause this effect to be even more significant.

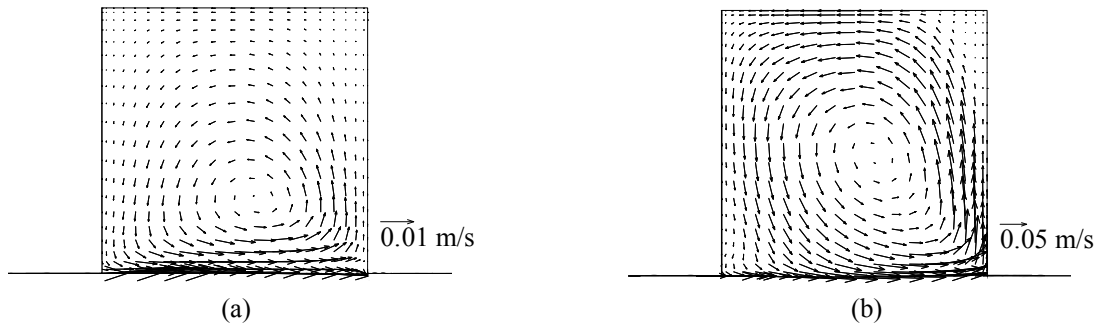


Figure 6. Flow pattern inside the grooves. (a) $Re = 10000$, (b) $Re = 50000$.

3.2. Results

Figure 7 shows comparisons involving the numerical friction factors obtained in the present work, where Fig. 7-(a) presents values from all four geometrical configurations listed in Tab. 1, for all six Reynolds numbers proposed, 6000, 10000, 20000, 30000, 40000 and 50000, and Fig. 7-(b) shows a comparison between the numerical friction factors obtained for configuration 4 in this work and experimental data of Morales *et al.* (2007). Blasius' smooth pipe correlation ($f_{smooth} = 0.316 \cdot Re^{-0.25}$) is plotted as well. Since the simulated Reynolds numbers range is somewhat short (6000-50000), a logarithmic scale would not be much useful, and variations can be more clearly seen in a standard conventional scale as shown.

From Fig. 7-(a), one can observe that, for a given Reynolds number, the friction factor increases through configurations 1 to 3, indicating that the friction factor increases with the increase of the groove length. Furthermore, the deviations between the numerical values for configurations 1 to 3 are more significant for higher Reynolds numbers, which can be clearly seen through Fig. 7-(a). As discussed for Fig. 6, when the Reynolds number increases, the momentum transfer between the groove and the outer flow is also increased, and this effect is amplified when the interface increases. Thus, it could be expected that deviations would tend to be bigger both for higher Reynolds numbers and for higher groove lengths, as can be seen in Fig. 7-(a). Note also from Fig. 7-(a) that, while increasing the groove length (made through configurations 1 to 2 and 2 to 3) induced notable increases on the friction factor, increasing the groove height (made through configurations 3 to 4) doesn't causes relevant variations on the friction factor. In fact, both 3 and 4 configurations consist of "d-type" roughness (according to many works, as Vijiapurapu & Cui [2007], "d-type" grooves are considered, in fact, cavities with the ratio between height and length lower than 4, i.e. not necessarily strictly square grooves), and as already discussed in the previous paragraph the phenomena involved with the variations here observed appear to be essentially related to the groove length and the Reynolds number.

From Fig. 7-(b), note that, especially for Reynolds numbers over 20000, the numerical results obtained show good agreement with experimental data. Significant deviations are observed, however, for Reynolds numbers lower than 20000, but Morales *et al.* (2007) reported some possible inaccuracies in this low range, due to an equipment limiting range for low mass flow rates. In fact, numerical results tend to the smooth pipe correlation for low Reynolds numbers, which is in agreement with one of the classic conclusions of Nikuradse (1933) work, who stated that for low Reynolds numbers the friction factor is basically a function of the Reynolds number, only.

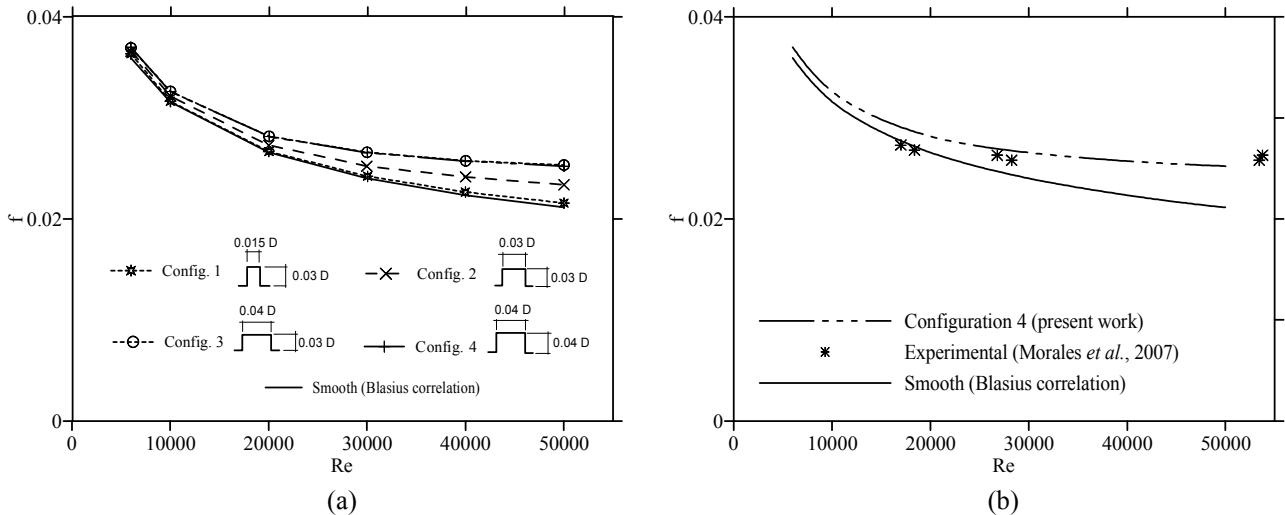


Figure 7. Numerical friction factors obtained, (a) for all geometric configurations and Reynolds numbers proposed, (b) for configuration 4 in comparison with experimental data (Morales *et al.*, 2007) and with smooth pipe Blasius' correlation.

According to Djenidi *et al.* (1994), a direct consequence of the momentum transfer enhancement discussed for Figs. 6 and 7-(a) is the increase of the Reynolds stress near the wall, which indirectly increases the friction coefficient, and hence also the global friction factor, a phenomenon well reflected by the results of Fig. 7-(a). In order to illustrate this phenomenon, Fig. 8 shows the Reynolds stress, $-\overline{v'w'}$ (where v' and w' are the radial and axial velocity fluctuations, respectively), normalized by the friction velocity proposed by Silberman (1980), $V_* = \sqrt{\Delta p D / 4 \rho L}$, for Reynolds 30000 (as an example) for all configurations, Fig. 8-(a), and for configuration 3 (also as an example) for all Reynolds numbers simulated, Fig. 8-(b).

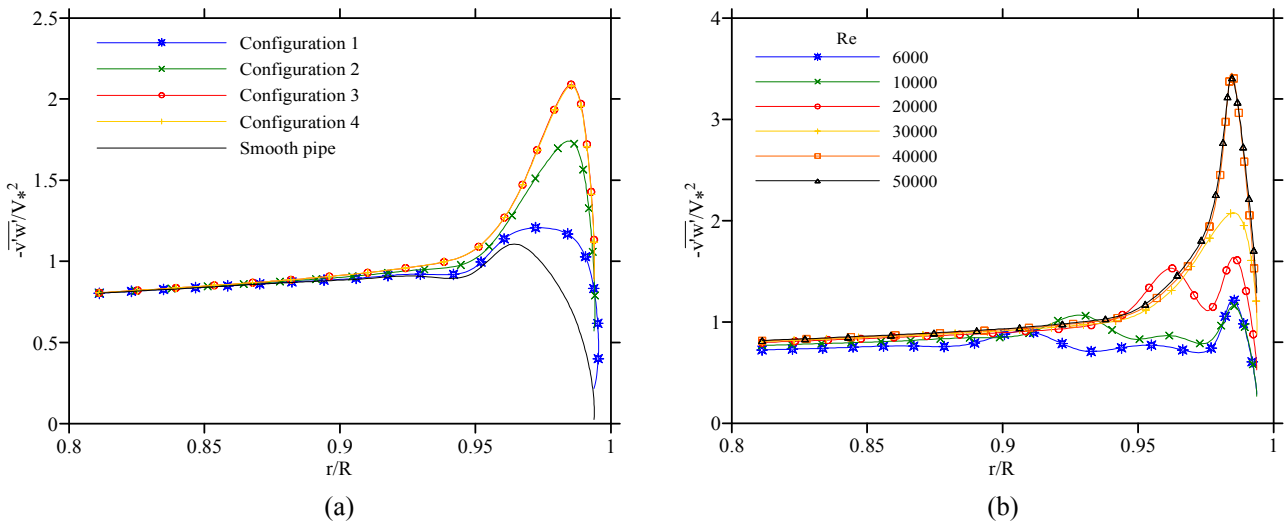


Figure 8. Dimensionless Reynolds shear stress near the wall. (a) Re 30000, for configurations 1 to 4 and smooth pipe; (b) Configuration 4, for Reynolds numbers from 6000 to 50000. Lines are fitting to the calculated data.

It can be clearly seen, through Fig. 8-(a), that when the groove length increases (which happens through configurations 1 to 3), the average Reynolds stress near the wall also increases. It is then expected that the global friction factor will increase if the groove length increases, and the increased Reynolds stress observed confirms this trend (since velocity fluctuations v' and w' tends to be intensified likewise, as a perturbation mechanism near the wall). Although exemplified just for $Re = 30000$, for all other Reynolds numbers this characteristic were observed. Figure 8-(b) shows that the Reynolds stress is also increased when the recirculation intensity is raised, which is provided here by increasing the Reynolds number, corroborating with the physical visualization in Fig. 6. Moreover, Figure 8-(a) numerically confirms, as observed in Fig. 7-(a), that increasing the groove height doesn't causes significant variations on the friction

factor if the groove shape still remains as a “d-type” cavity, since Reynolds stress plots are almost identical for configurations 3 and 4.

3. CONCLUSIONS

The present paper numerically investigated the influence of corrugated surfaces on the friction factor in circular cross section ducts. Four geometric configurations were assumed, involving variations on grooves length and height, and a numerical analysis was carried on for Reynolds numbers from 6000 to 50000. In general, it was found that the friction factor increases for a given Reynolds when the grooves length increases, and the friction factor also increases for a given cavity shape when the Reynolds number increases. This trend is a result of a momentum transfer enhancement between the confined recirculation in the groove and the outer flow, and was confirmed by a numerical analysis of the Reynolds shear stress near the wall, for which could be observed that velocity fluctuations are intensified near the wall when the momentum transfer between the groove and the outer flow increases, indirectly providing a increase in the friction factor, as discussed. The numerical results shows good agreement with experimental data for Reynolds numbers over 20000, but some deviations were found for low Reynolds numbers, due to an equipment limiting range for low mass flow rates reported by Morales *et al.* (2007). Aside of that, numerical results agree with the conclusion of Nikuradse (1933) of roughness non-dependence for low Reynolds numbers.

4. ACKNOWLEDGEMENTS

The authors acknowledge the financial support from the National Agency for Petroleum, Natural Gas and Biofuels (ANP) through its Human Resources Program in UTFPR (PRH-10), CAPES and from PDP/TE/CENPES/PETROBRAS.

5. REFERENCES

- Chen, J.J., Leung, Y.C., Ko, N.W., 1986, “Drag Reduction in a Longitudinally Grooved Flow Channel”, *Industrial and Engineering Chemistry Fundamentals*, Vol. 25, pp. 741-745.
- Djenidi, L., Anselmet, F., Antonia, R.A., 1994, “LDA measurements in a turbulent boundary layer over a d-type rough wall”, *Experiments in Fluids*, Vol. 16, pp. 323-329.
- Dong, Y., Huixiong, L., Tingkuan, C., 2001, “Pressure Drop, Heat transfer and Performance of Single-Phase Turbulent Flow in Spirally Corrugated Tubes”, *Experimental Thermal and Fluid Science*, Vol. 24, pp. 131-138.
- Jiménez, J., 2004, “Turbulent Flows over Rough Walls”, *Annual Review of Fluid Mechanics*, Vol. 36, pp. 173-196.
- Kennedy, J.F., Hsu, S.T., Lin J.T., 1973, *Journal of the Hydraulics Division, Proceedings of the American Society of Civil Engineers*, Vol. 99, pp. 605-616.
- Liu, S.K., Klein, S.J., Johnstone, J.P. 1966, Report MD-15, Stanford University: Stanford, CA.
- Morales, R.E.M., Franco, A.T., Junqueira, S.L.M., Erthal, R.H., 2007, “Experimental Analysis of Turbulent Flow in Flexible Pipes” Technical Report - UTFPR/CENPES-PETROBRAS, Curitiba, 2007.
- Nikuradse, J., 1933, “Laws of flow in rough pipes”, VDI Forschungsheft 361, NACA TM 1292, 1950.
- Patankar, S.V., 1980, “Numerical Heat Transfer and Fluid Flow”. Philadelphia: Taylor & Francis.
- Patankar, S.V., Liu, C.H., Sparrow, E.M., 1977, “Fully Developed Flow and Heat Transfer in Ducts Having Streamwise-Periodic Variations of Cross-Sectional Area”, *Journal of Heat Transfer, Transactions of the ASME*, Vol. 99, pp. 180-186.
- Perry, A.E., Schofield, W.H., Joubert, P.N., 1969, “Rough wall turbulent boundary layers”, *Journal of Fluid Mechanics*, Vol. 37, pp. 383-413.
- Silberman, E., 1970, “Effect of Helix Angle on Flow in Corrugated Pipes”, *Journal of the Hydraulics Division, Proceedings of the American Society of Civil Engineers*, Vol. 96, N° HY11, pp. 2253-2263.
- Silberman, E., 1980, “Turbulence in Helically Corrugated Pipe Flow”, *Journal of the Hydraulics Division, Proceedings of the American Society of Civil Engineers*, Vol. 106, N° EM4, pp. 699-717.
- Spalding, D.B., 1994, “The PHOENICS Encyclopedia”, London: CHAM Ltda.
- Vijapurapu, S., Cui, J., 2004, “Simulation of Turbulent Flow in a Ribbed Pipe Using Large Eddy Simulation”, *Numerical Heat Transfer, Part A*, Vol. 51, pp. 1137-1165.
- Walsh, M.J., Weinstein, L.M., 1979, “Drag and Heat-Transfer Characteristics of Small Longitudinally Ribbed Surfaces”, *AIAA Journal*, Vol. 17, pp. 770-771.

5. RESPONSIBILITY NOTICE

The authors are the only responsible for the printed material included in this paper.